Front. Earth Sci. 2024, 18(2): 364–383
https://doi.org/10.1007/s11707-022-1067-1

RESEARCH ARTICLE

Paleoenvironment evolution and organic matter enrichment mechanisms in the first member of the Qingshankou Formation, Songliao Basin, China

Ying LI[1,2], Min WANG (✉)[1,2], Yu YAN[1,2], Xin WANG[1,2], Jinyou ZHANG[3], Xuefeng BAI[4], Yuchen ZHANG[1,2], Jiaheng XUE[5], Junsheng FEI[1,2], Lianbin ZHANG[1,2], Guojun WANG[3]

1 School of Geoscience, China University of Petroleum (East China), Qingdao 266580, China
2 Shandong Provincial Key Laboratory of Deep Oil and Gas, Qingdao 266580, China
3 Exploration and Development Research Institute of Daqing Oilfield Co Ltd., Daqing 163712, China
4 Exploration Division, PetroChina Daqing Oilfield Company, Daqing 163453, China
5 Department of Physics, Xiamen University Malaysia, Bandar Sunsuria 43900, Malaysia

Abstract Organic matter is the basis for oil and gas generation, and the depositional environment controls its enrichment. The first member of the Qingshankou Formation (K_2qn^1) in Songliao Basin has a thick organic-rich shale and so is an important target section for shale oil exploration and development. In the Gulong Sag, shale samples from this unit were collected over the full length of the section. The characterization of the environments of deposition (EOD) of K_2qn^1 was improved by utilizing lithological characteristics, thin section observations, elemental compositions, and organic carbon concentrations. Combined with the normalization coefficients proposed in this paper, an organic matter correlation model was established to elucidate the factors that influence organic matter enrichment. From the bottom to the top of K_2qn^1, the lake depth gradually becomes shallower, the primary productivity first decreases and then increases, the reducing conditions become stronger and then weaker, the water salinity gradually decreases, the climate first becomes semi-humid and then warm and humid, and the input of terrigenous debris first decreases and then increases. A major marine transgression at the base of the K_2qn^1's brought in nutrients to increase primary productivity, and the density-stratified reducing environment preserved and enriched organic matter. High primary productivity occurred during the middle of the deposition of the K_2qn^1, while terrigenous input is low. Organic matter is preserved in reduced deep lake environments, resulting in organic matter-rich black shale. The lake became shallower, and the salinity decreased in the upper part of K_2qn^1. Benthic organisms rapidly multiplied, consuming large amounts of oxygen and destroying the previously depositional environment, resulting in a reducing environment disturbed by benthic organisms with poor preservation conditions and the lowest organic matter content.

Keywords major and trace elements, paleoenvironment evolution, OM enrichment mechanism, lacustrine shale, Songliao Basin, Qingshankou Formation

1 Introduction

Since the shale gas revolution in North America, unconventional oil and gas resources have become a major focus of global exploration (Jarvie, 2012). The Songliao Basin is the largest Cretaceous continental sedimentary basin in Asia and is a major source of petroleum, including the Daqing and Jilin oilfields (Zou et al., 2019; Guan et al., 2021). The Qingshankou Formation is a major oil-producing formation in the Songliao Basin and has thick, organic-rich black shale that offer excellent shale oil exploration prospects (Liu et al., 2019; Sun et al., 2021). Sufficient organic matter is a prerequisite for oil and gas generation, and the depositional environment (EOD) controls its enrichment (Peters et al., 1986; Hakimi et al., 2014). To encourage unconventional oil and gas exploration and production, it is essential to study the depositional environment evolution and organic matter enrichment mechanisms (Zhao et al., 2020).

The Qingshankou Formation is a lacustrine environment and several studies have been done previously to

Received February 1, 2023; accepted May 12, 2023

E-mail: wangm@upc.edu.cn

reconstruct the Qingshankou Formation's shale sedimentary environments. Based on spore-pollen data, Huang et al. (1999) found that evergreen broad-leafed forests, representing a warm-humid environment, were prevalent during the deposition of the Qingshankou Formation. According to Wang et al. (1996), the intrusion of seawater during the deposition of the Qingshankou Formation caused the lake water to stratify, resulting in the formation of black shale in a stably stratified lake environment. Hou et al. (2003) determined occurrences of anoxic episodes and marine transgression events in the Cretaceous Songliao Basin, particularly at the base of the Qingshankou Formation, where reducing conditions were strong. Wu et al. (2008) established a floating astronomical time scale for the Qingshankou Formation and determined that the paleolake anoxic event occurred close to the Cretaceous Oceanic Anoxic Event 2 (OAE2). Feng et al. (2011) studied the sedimentary biomarkers and observed that K_2qn^1 lake water was highly saline and stratified.

Numerous academics have studied the evolutionary features of the sedimentary environment and organic matter enrichment mechanisms in K_2qn^1 in recent years. According to Wang et al. (2015), in K_2qn^1, shore-shallow lakes with oxygenated water and high energy hydrodynamics had poor organic matter preservation conditions, while semi-deep and deep lakes had favorable preservation conditions. Good preservation conditions with low energy hydrodynamic conditions and a strongly reducing environment promote organic matter enrichment in K_2qn^1. Wang et al. (2019) used thin section observations and geochemical data analysis to show that the organic matter in K_2qn^1 was deposited in a reducing environment with low energy hydrodynamics, but that the reducing environment was disturbed when terrigenous debris input increased, implying that terrigenous debris input was also an important control factor for organic matter enrichment in K_2qn^1. However, Song et al. (2016) noted that the enrichment of organic materials in K_2qn^1 is not only controlled by preservation conditions but also by high primary productivity. Stratified reducing conditions with high primary productivity and salinity jointly control the enrichment of organic matter in K_2qn^1. According to elemental and biomarker compound analysis, Zheng et al. (2020) also found that organic matter abundance is highest when primary productivity is highest and reducing conditions are the most intense, and that high salinity also influences organic matter enrichment in K_2qn^1. Furthermore, Fu et al. (2022) suggested that under a warm and humid climate, high salinity, high primary production, and weak terrigenous debris input enriched organic matter in K_2qn^1, and the reducing environment was not a major controlling factor.

In summary, there is still no agreement on the major controlling factors of organic matter enrichment in K_2qn^1. Previous research focused on primary productivity and redox conditions with little consideration of other factors. Currently, the studies of the paleoenvironmental features of K_2qn^1 only characterize lake water depth, salinity, or redox conditions. Few studies have completely investigated the paleoenvironment of deposition, including the redox conditions, water salinity, paleoclimate, terrigenous debris input, primary productivity, and water depth. Consequently, based on lithological characteristics, thin section observation, elemental composition, and organic carbon abundance data, this study aims to: 1) provide a detailed description of the paleoenvironment features (including redox conditions, water salinity, paleoclimate, terrigenous debris input, and water depth) in K_2qn^1; 2) establish the TOC correlation model with comprehensive multi-factor control and comprehensively analyze the effects of various factors influencing the enrichment of organic matter in K_2qn^1 in order to provide a reference for the study of shale organic matter enrichment in the Songliao Basin and new geochemical evidence for shale oil exploration.

2 Geological setting

The Songliao Basin is located in north-east China and has an area of approximately 26×10^4 km^2. It is one of the most prolific terrestrial basins in terms of oil and gas resources in the world. The basin is divided into six structural units: the northern plunge, the central depression, the north-eastern uplift, the south-eastern uplift, the south-western uplift, and the western slope (Fig. 1(a)). The major oil and gas producing area is the central depression, including the Qijia-Gulong sag, Daqing placanticline, Sanzhao sag, Changling sag, and the Chaoyanggou terrace (Feng et al., 2010, 2021). The focus of the research is the Gulong Sag, which is west of the central depression in the Songliao Basin.

The basin contains Jurassic, Cretaceous, Eogene, and Neogene clastic deposits (Li, 1996). The Cretaceous sedimentary period was one of the warmest periods of the Phanerozoic, when significant oceanic anoxic events (OAEs) occurred globally (Jenkyns, 1980; Wu et al., 2009). Upper Cretaceous formations include Qingshankou, Yaojia, Nenjiang, Sifangtai, and Mingshui (Fig. 2) (Gao and Cai, 1997). The occurrences of marine transgressive events during this time have been demonstrated by paleontology, geochemistry, and other geological techniques (Gao et al., 1992; Hou, 1999; Feng et al., 2009). A warm and humid climate during the Turonian–Coniacian period promoted aquatic organism blooms, and widespread water column stratification with bottom water anoxia favored organic matter preservation, resulting in the deposition of organic matter-rich layer series in large parts of the Songliao paleolake at that time (Fig. 2) (Xu et al., 2015).

The Qingshankou Formation is a favorable stratum for the development of the Gulong and Gaotaizi oil layers, and its seismic reflection horizons are T_2 and T_1^1, which correspond to the bottom and top surfaces (Figs. 1(c) and 2). Based on lithology, the Qingshankou Formation is

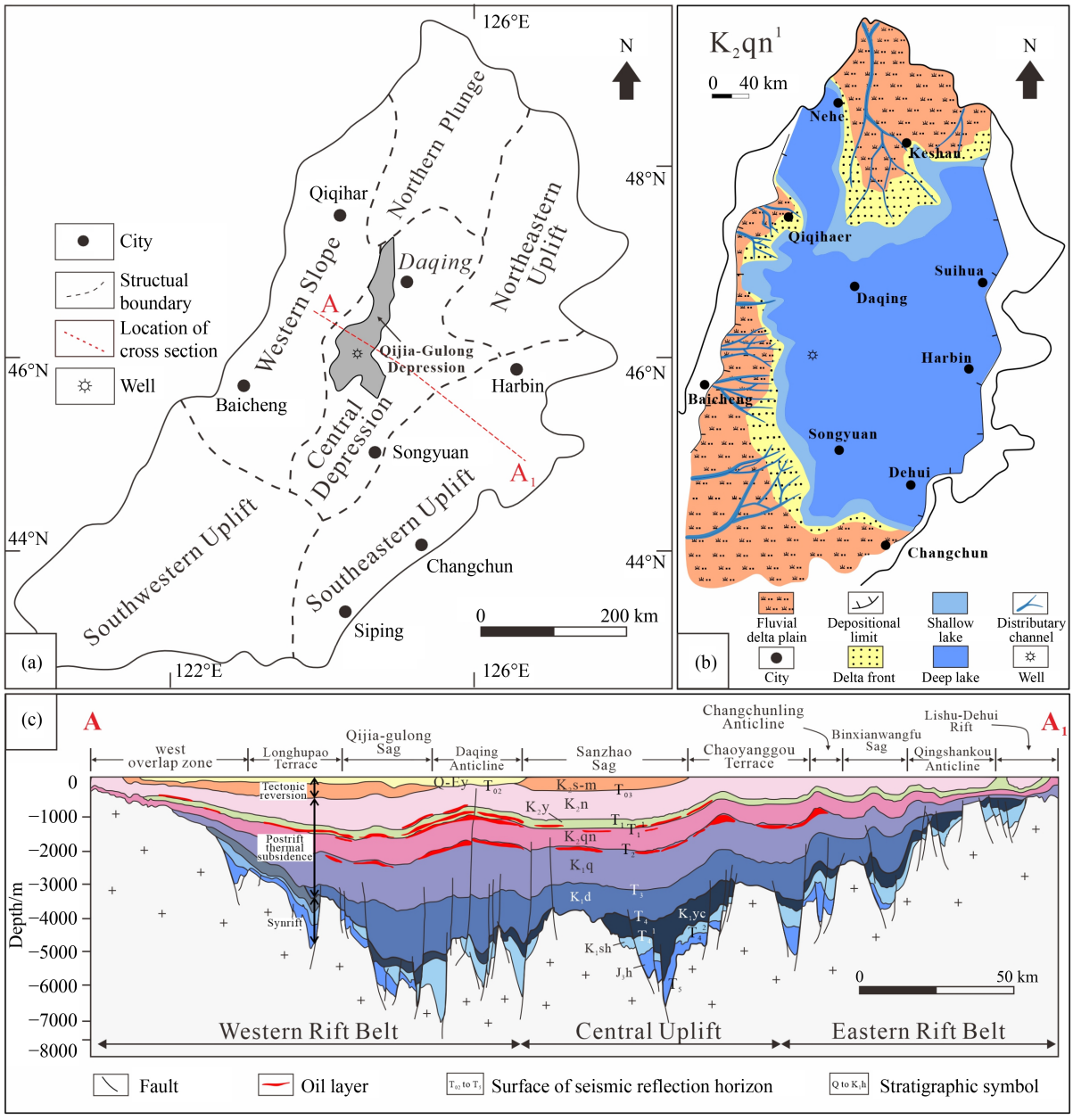

Fig. 1 (a) Structural elements of the Songliao Basin (modified after Feng et al., 2010). (b) Areal distribution of sedimentary facies during K_2qn^1 deposition in the Songliao Basin (modified after Feng et al., 2010). (c) Songliao Basin geologic profile, location shown in Fig. 1(a) A-A1 (modified after Fu et al., 2022).

classified into three units (K_2qn^1, K_2qn^2, and K_2qn^3). Large-scale marine transgression occurred during the depositional period of K_2qn^1, and the lake basin area reached its maximum. The semi-deep lacustrine-deep lacustrine facies was formed in this period (Fig. 1(b)), and its lithology is mainly large sets of dark shale and oil shale, with thin dolomite, siltstone, muddy siltstone, and shell limestone interlayers (Fig. 2). Organic rich shales in K_2qn^1 are the main oil source rock, with high OM abundance. The R_o of the organic rich shales lies between 1.0%−1.6% in the main depression region, which could be a key shale oil exploration target (Liu et al., 2022). The central depression area, in particular, is the most developed high-quality source rock and a favorable interval for Gulong shale oil exploration and development (Sun et al., 2021). In 2021, Daqing Oilfield discovered the K_2qn^1 shale oil reservoir in Gulong Sag, with an oil-bearing area of 1413 km^2 and a predicted reserve of 12.68×10^8 t (Li et al., 2022).

3 Materials and methods

To study the evolution of the depositional environments in the K_2qn^1, samples were taken through the entire interval in Well G (Fig. 1(a)), with a depth range of

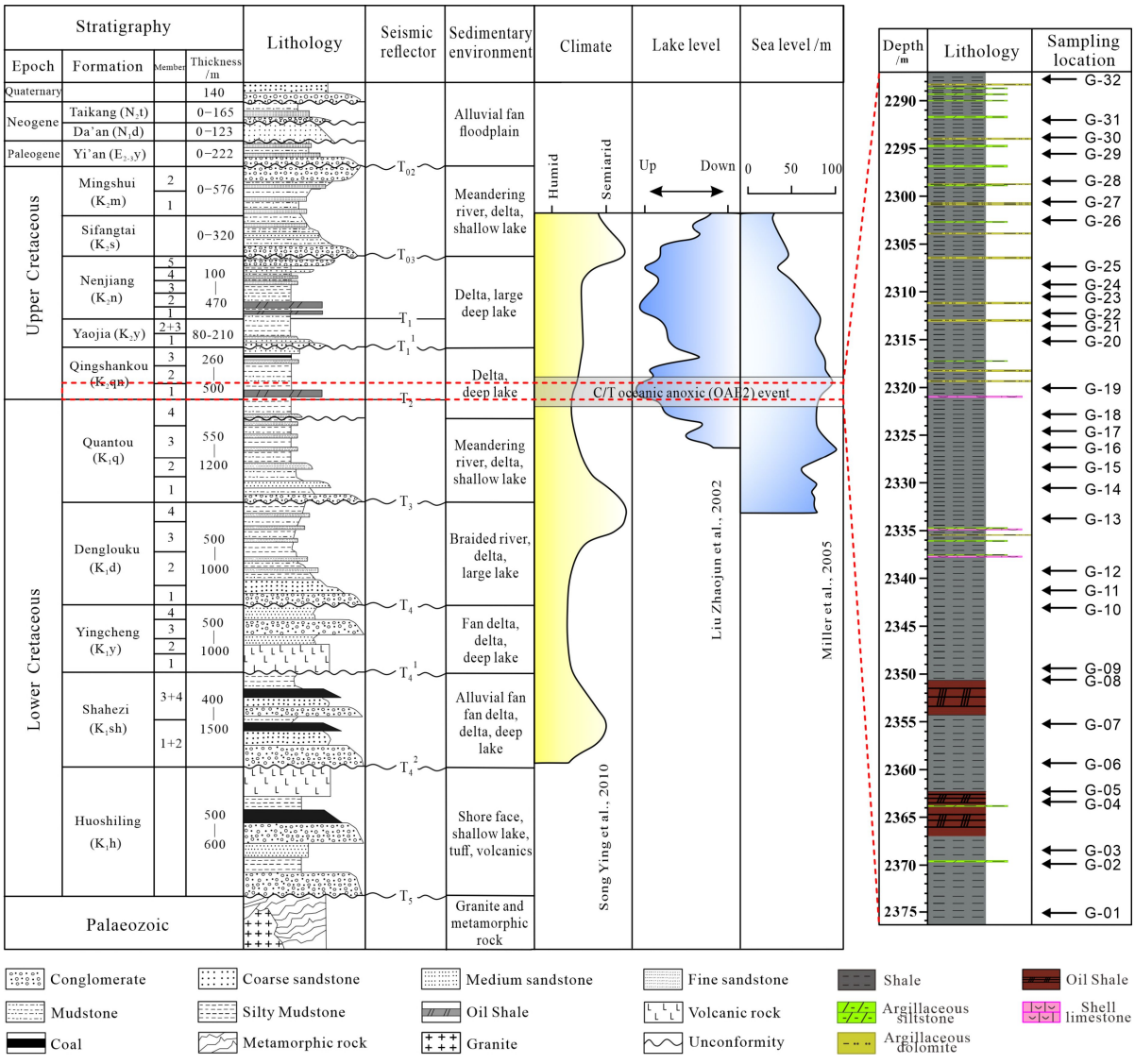

Fig. 2 Integrated stratigraphic column of the Songliao Basin (modified according to Xu et al., 2015; Fu et al., 2022).

2287–2377 m (Fig. 2). A total of 133 samples were analyzed for TOC content and 32 samples for elemental content. After sampling, all core samples were stored in plastic bags to ensure as little contamination and oxidation as possible.

Total organic carbon (TOC) content analyses were all performed by an Eltre CS580A-type carbon and the experimental process was based on the national standard GB/T 19145-2003. The accuracy of the analysis was greater than 0.5%. The major, trace, and rare earth element (REE) concentrations for the shale samples were measured at 14°C and 30% relative humidity. All samples were crushed below 200 mesh for further examination. The melt sheet method and X-ray fluorescence spectrometry (XRF) were used for quantitative element analysis. Approximately 0.7 g of sample powder was baked in a muffle furnace at 1000°C for 3−5 h before being mixed with 7.7 g of anhydrous $Li_2B_4O_7$ solvent. After that, the Analymate-V4D melting apparatus formed a melting sheet that was measured by an Epsilon 3XLE X-ray fluorescence spectrometer. The experimental process was based on GB/T 14506.28-2010 and GB/T 14506.14-2010, with an analytical error of less than 5%. Trace elements and REE were dissolved by mixed acid closed digestion and measured by inductively coupled plasma mass spectrometry (ICP-MS). The experimental process was based on the national standards GB/T 14506.30-2010 and GB/T 14506.11-2010, with an analytical error of less than 5%.

4 Results

4.1 Shale properties

The TOC content of K_2qn^1 shale samples gradually decreases from bottom to top (Fig. 3), while the total concentrations vary from 0.70% to 4.94%, with an

average value of 1.84%. The TOC concentrations in the lower, middle, and upper portions of K_2qn^1 exhibit a regular pattern of first increasing, and subsequently decreasing, demonstrating a cyclic characteristic. The lithology of K_2qn^1 is dominated by black shale; nevertheless, in the lower, middle, and upper parts of K_2qn^1, the lithofacies assemblages show substantial variation. The lower sedimentary section is dominated by black shale and oil shale, and the oil shale deposits correspond to the sections with the most enriched TOC content. The central sedimentary section contains mostly black shale deposits, which indicates a depositional environment with few or no benthic organisms. The upper sedimentary section is significantly different from the central section since the upper black shale is intercalated with several thin layers of argillaceous siltstone and dolomite (Fig. 3).

4.2 Major, trace, and REE concentrations

Appendix A lists major element analytical results. Analysis of the major elements show that SiO_2 and Al_2O_3 are the most abundant constituents (Fig. 4(a)). Higher concentrations of K_2O compared to Na_2O (Fig. 4(a)) indicate more K-feldspar or K-bearing minerals. Ti is not affected by diagenetic processes and its oxide (TiO_2) correlates with Al_2O_3, indicating a consistent source of detrital material in K_2qn^1 (Fig. 4(b)). Appendix B contains trace element analysis results. Normalized to post-Archean Australian shale (PAAS) (Taylor and McLennan, 1985) and plotted on a line plots (Fig. 4(c)), trace elements show consistent distribution patterns, indicating that K_2qn^1 may have the same sedimentary provenance, with significant differences only at the contact of the Qingshankou and Quantou Formations (Figs. 2 and 4(c)). The rare earth elements (REE) distribution is similar, among which the light rare earth elements (LREE) mainly include La, Ce, Pr, Nd, Pm, Sm, and Eu, with negative Eu anomalies (Fig. 4(d)). The heavy rare earth elements (HREE) mainly include Gd, Tb, Dy, Ho, Er, Tm, Yb, Lu, and Y. The light rare earth elements are substantially enriched, while the heavy rare earth elements are distributed more evenly, with a smaller difference. The formula for calculating $(La/Yb)_N$ is $(La/Yb)_N = (La/Yb)_{sample}/(La/Yb)_{chondrite}$, where $(La/Yb)_{sample}$ is the La/Yb ratio of the sample and $(La/Yb)_{chondrite}$ is the La/Yb ratio of the chondrite standard (Taylor and McLennan, 1985). In this paper, the calculated $(La/Yb)_N$ varies from 7.70 to 11.58, clearly indicating the difference between LREE and HREE.

4.3 Formation subdivision characteristics

Terrigenous debris input affects (e.g., dilutes or enhances) the sediment's authigenic major and trace element concentrations. To eliminate the influence of terrigenous debris, enrichment factors (EFs) can be used to define element enrichment or depletion (Tribovillard et al., 2006), which are calculated as follows:

$$X_{EF} = (X/Al)_{sample}/(X/Al)_{averageshale}, \quad (1)$$

where X is the element to be calculated and the post-Archean Australian shale (PAAS) is used for the average shale. If $X_{EF} > 1$, the element is enriched relative to the PAAS while if $X_{EF} < 1$, the element is depleted.

The EF values of nine major elements and 16 trace elements are displayed in Fig. 3. From bottom to top, the EF values of each element in the first member of the

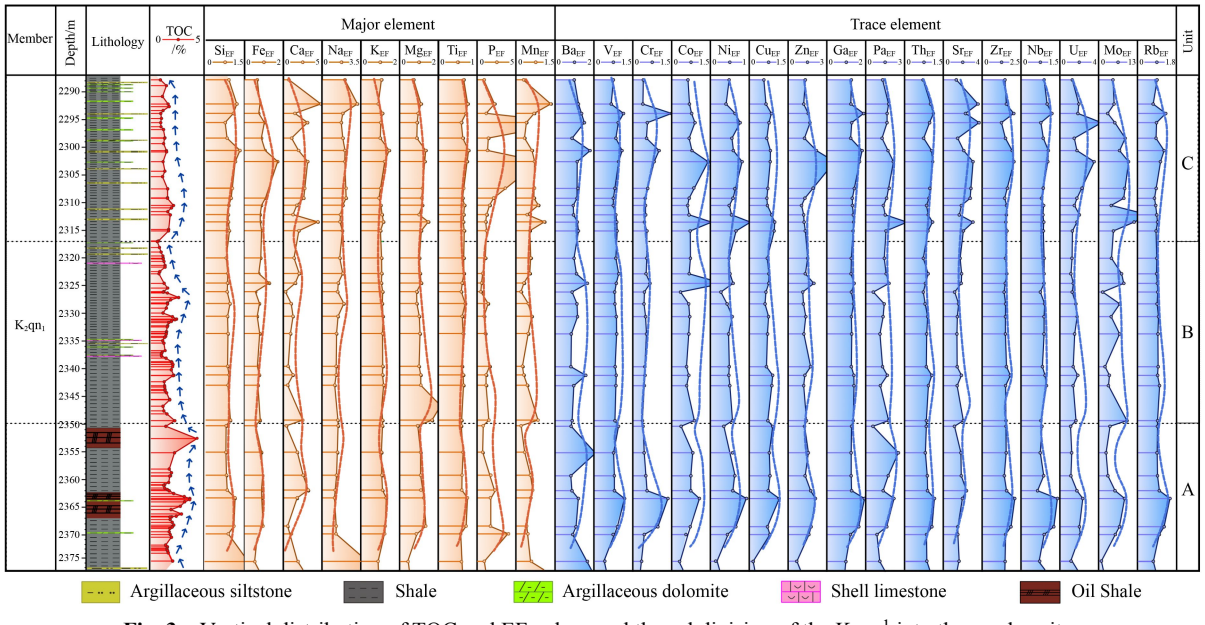

Fig. 3 Vertical distribution of TOC and EF values and the subdivision of the K_2qn^1 into three sub-units.

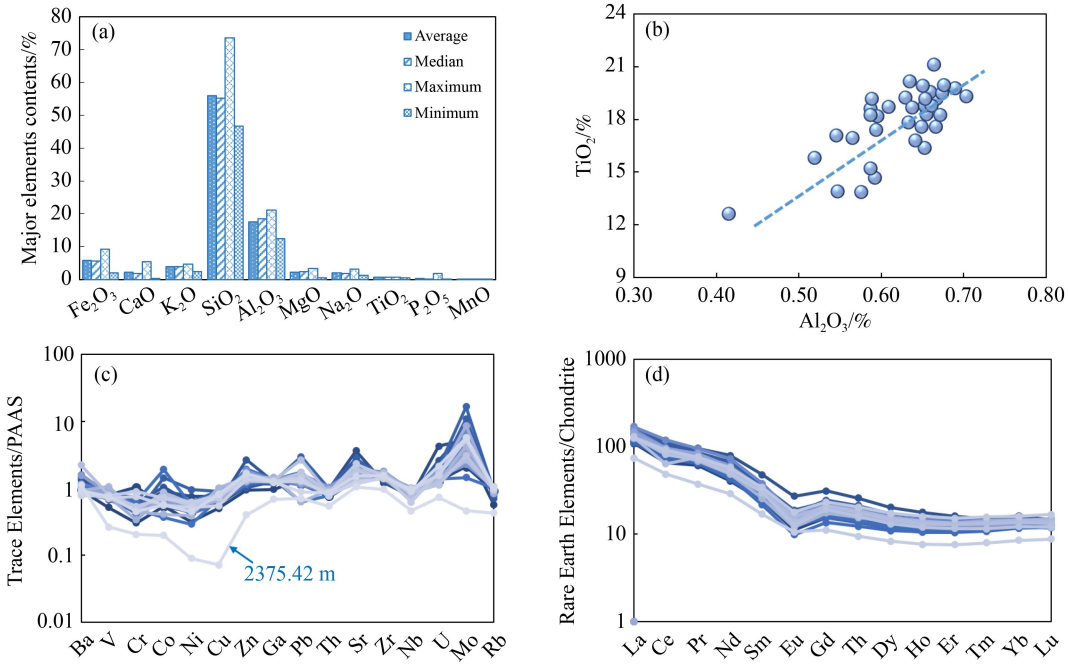

Fig. 4 (a) Concentrations of major elements; (b) relation of Al_2O_3 to TiO_2; (c) PAAS-normalized trace element line plots; (d) REE distribution patterns normalized to chondrite.

Qingshankou Formation show stages of regular cyclic increases and decreases (Fig. 3). K_2qn^1 is a third-order sequence that contains, from bottom to top, a transgressive system tract (TST), highstand system tract (HST), and regressive system tract (RST) (Jia et al., 2013). By comparing the differences in the lithofacies assemblages of the three system tracts and the cyclic features of the TOC content (Fig. 3) indicate that the first member of the Qingshankou Formation can be further divided into three units, from bottom to top: Unit A, Unit B, and Unit C (Fig. 3).

Unit A has the highest TOC content, with a maximum of 4.94%; Unit B has a moderately high TOC content, with an average of 1.74% and a maximum of 2.98%; and Unit C has the lowest TOC content, with an average of 1.54%. Relative to the PAAS, Ca, Na, K, and P are enriched, while Fe, Ti, and Mn are depleted in all three units (Fig. 5(a)). High Ca content may be due to calcite and abundant bivalves or gastropod fossils. Ba, Zn, Ga, Pb, Sr, Zr, U, and Mo are enriched, while V, Cr, Co, Ni, Cu, Th, Rb, and Nb are depleted in all three units (Fig. 5(b)). All elements show consistent enrichment characteristics, indicating that the three units may have the same sedimentary provenance.

5 Discussion

5.1 Primary productivity and paleoenvironment evolution

5.1.1 Primary productivity evolution

Phosphorus (P) is a structural element of Deoxyribo Nucleic Acid (DNA), ribonucleic acid (RNA), and many biomolecules, which are essential components of living organisms (Haddad and Martens, 1987); uranium (U) is preserved in a reduced environment by complexation with trace elements contained in primary producers, so U

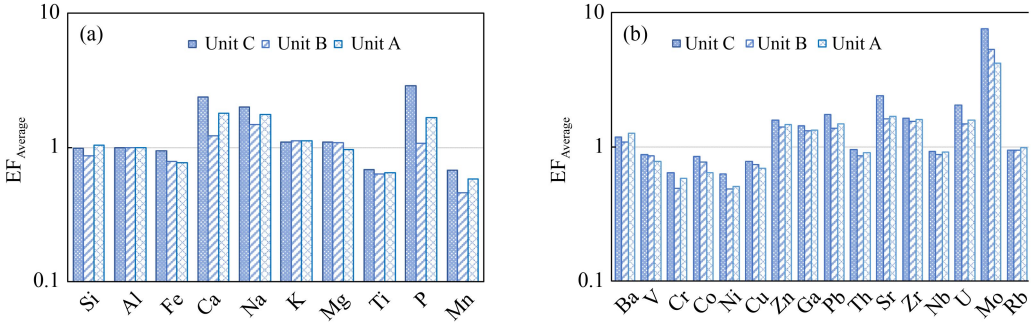

Fig. 5 Average EF values ($EF_{average}$) in three K_2qn^1 units. (a) $EF_{average}$ of major elements; (b) $EF_{average}$ of trace elements.

can be used to restore primary productivity under reducing conditions (Chase et al., 2001; Yang and Yu, 2002). When P and U are present as biological phosphorus (P_{bio}) and biological uranium (U_{bio}), they can be used to restore the primary productivity. The formula for P_{bio} is

$$w(P_{bio}) = w(P_t) - w(Al_t) \times (w(P)/w(Al))_{PAAS}, \quad (2)$$

where (P_{bio}) is biological phosphorus, (P_t) is total phosphorus in the sediment, (Al_t) is total aluminum in the sediment, and $(w(P)/w(Al))_{PAAS}$ is the ratio of phosphorus to aluminum in PAAS. U_{bio} is calculated in the same way.

P_{bio} is mostly positive, with an average of 0.07%; U_{bio} is all positive, ranging from 0.18% to 10.11%, with an average of 2.14%, indicating high primary productivity. In Units A, B, and C, primary productivity all showed a regular evolution of increasing and then decreasing (Fig. 6(b)). Units A and C have relatively high P_{bio} and U_{bio}, indicating relatively high primary productivity. From the bottom to the top of K_2qn^1, primary productivity fell then rose (Figs. 7(a) and 7(b)).

Influenced by the global sea level rise of late Albian (112–97 Ma) (Jenkyns, 1980), a large-scale transgression occurred during the K_2qn^1, which was a reduction environment of semi-deep lake and deep lake. During this period, two slight uplift-subsidence processes occurred, and the delta advanced in different directions to the lake basin, forming a lithological combination of thick black mudstone/shale, with gray siltstone and fine sandstone (Liu et al., 2018). The lake became connected to the marine environment during the K_2qn^1, and the invading seawater not only provided nutrients but also changed the lake's physicochemical properties (Xu et al., 2021). A large number of ostracod fossils were deposited in the Qingshankou Formation, among which the freshwater ostracods have strict salinity limits (Carbonel et al., 1988). A large-scale marine transgression occurred in Unit A, which resulted in a major die-off of freshwater organisms due to salinity intolerance. Simultaneously, the nutrients carried by seawater cause plankton blooms, which resulted in high primary productivity in Unit A. The scale of marine transgression decreased in Unit B, and the nutrient input from the seawater incursion was lower than in Unit A. Meanwhile, saline lake water limited the freshwater organisms' survival and reproduction, lowering primary productivity. According to Wang et al. (1994), during the first marine transgression in the Songliao Basin, conchostracan genera and species were relatively rare at the base of the K_2qn^1, but after the marine transgression, conchostracans quickly propagated in large quantities, and there was a rapid increase in conchostracan genera and species. In Unit C, lake organisms basically had adapted to the fresh and brackish water and evolved new genera and species, resulting in a rebound in primary productivity.

5.1.2 Paleoenvironment evolution

1) Redox conditions

Trace elements like V, Cr, and Ni will mainly be

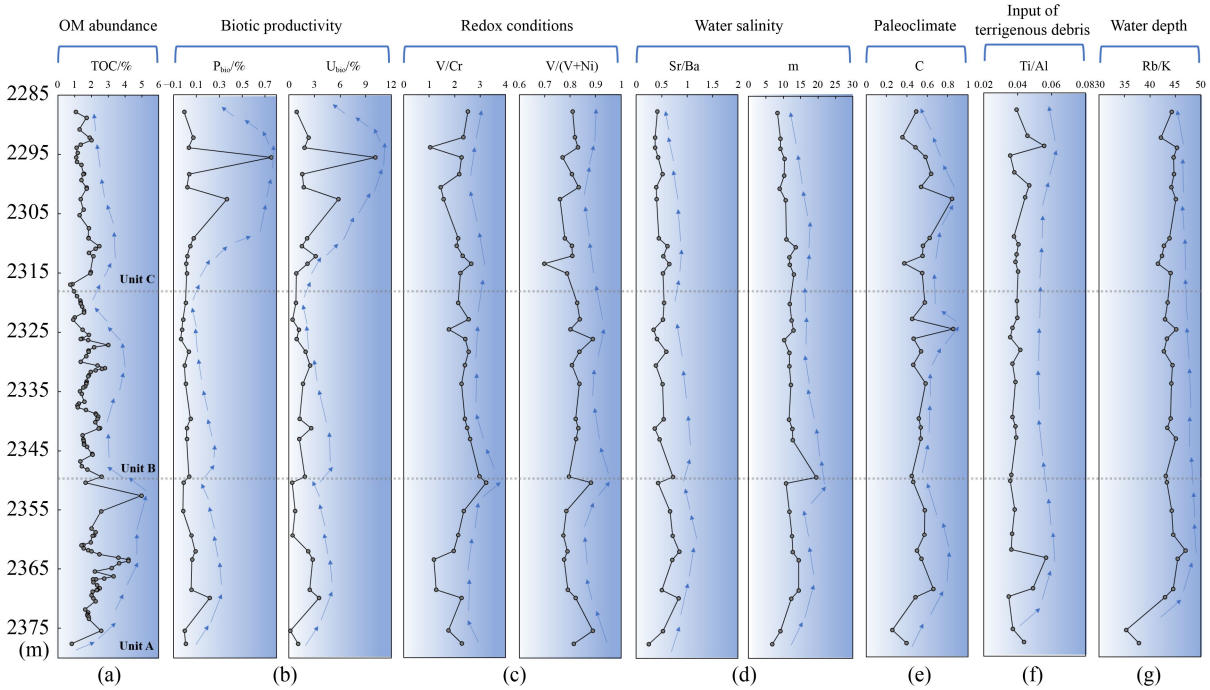

Fig. 6 Vertical variations in (a) OM abundance, (b) biotic productivity, (c) redox conditions, (d) water salinity, (e) paleoclimate, (f) terrigenous debris input, and (g) water depth, with darker colors representing larger indicator values in the figure.

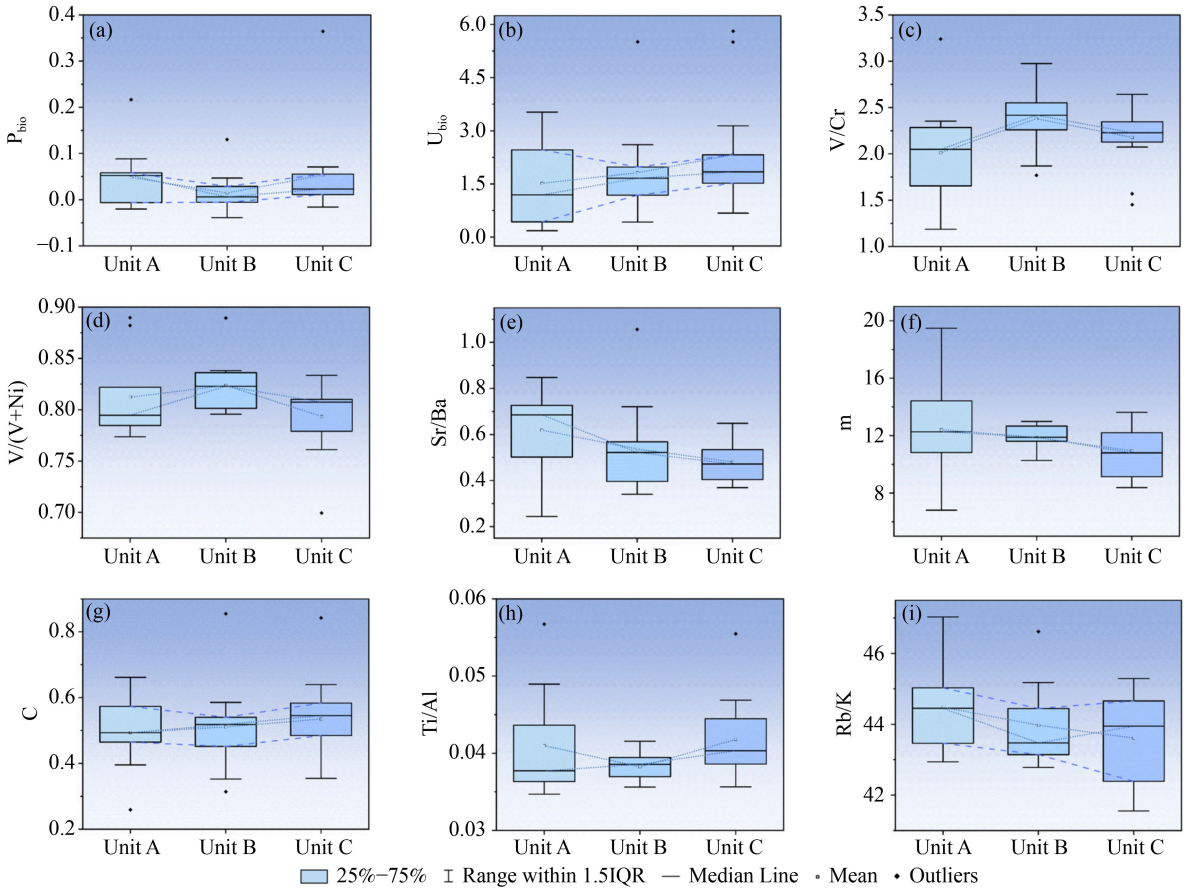

Fig. 7 Primary productivity features are characterized by (a) P_{bio} and (b) U_{bio}; the redox conditions are characterized by (c) V/Cr and (d) V/(V+Ni); the salinity features are characterized by (e) Sr/Ba and (f) m-value; the paleoclimate features are characterized by (g) C-value; the terrigenous detrital input is characterized by (h) Ti/Al; and the water depth features are characterized by (i) Rb/K.

adsorbed by colloidal particles or clay and then deposited. The rate of deposition of V is higher than Ni and is more efficient than that of Cr in reducing conditions, so V/Cr and V/V + Ni can be used to indicate the redox status (Wignall, 1994; Rimmer et al., 2004; Wang et al., 2017). Ratios of V/Cr > 4.25, V/Cr between 2 and 4.25, and V/Cr < 2 indicates anoxic, suboxic to dysoxic, and oxic environments respectively (Jones and Manning, 1994); V/(V + Ni) > 0.84, V/(V + Ni) between 0.6 and 0.84, and V/(V + Ni) < 0.6, indicated anoxic, dysoxic, and oxic environments respectively (Dill, 1986; Zhang et al., 2012).

The first member of the Qingshankou Formation has a small but variable range of redox conditions, from suboxic to dysoxic (Fig. 6(c)). Unit B has the highest V/Cr and V/(V + Ni) ratios, indicating the strongest reducing environment. From K_2qn^1's bottom to top, the reducing conditions became stronger and then weakened (Figs. 7(c) and 7(d)). When the marine transgression occurred in K_2qn^1, the oxygen-enriched surface seawater flowed into the lake, causing a lessening of the severity of the dysoxic conditions in Unit A. Bioturbation can disrupt the depositional environment. The occurrence of bioturbation in Unit C is evident from the thin section observations (Figs. 8(a) and 8(b)), demonstrating that following the primary productivity recovery, the bioturbation in Unit C's bioturbation will disrupt the environment.

2) Lake water salinity

The trace element ratio Sr/Ba has been widely used in paleosalinity restoration (Vincent et al., 2006). Sr/Ba greater than 1.0 indicates saline water, Sr/Ba between 0.5 and 1.0 indicates brackish water, and Sr/Ba less than 0.5 indicates fresh water (Rimmer, 2004). In addition, the element Mg occurring in sea water and the terrestrial element Al can be used as indicators of paleosalinity. The ratio of the concentrations of the two oxides is defined as the *m*-value, and a higher *m*-value indicates a higher salinity (Zhang, 1988; Chen et al., 1997), which is calculated as

$$m = 100 \times (\mathrm{MgO}/\mathrm{Al_2O_3}). \quad (3)$$

The lake water salinity decreases from bottom to top in K_2qn^1, mostly showing a brackish water environment (Fig. 6(d)), with the highest Sr/Ba ratio and m-value in Unit A, followed by Unit B, and the lowest in Unit C, indicating the lowest salinity in Unit C (Figs. 7(e) and 7(f)). The influx of seawater during deposition of Unit A

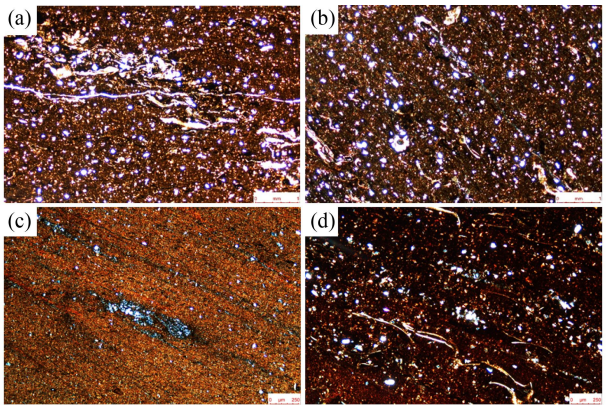

Fig. 8 Microscopic characteristics of samples in K_2qn^1. Single-polarized microscope images, (a) felsic clastic deposition, 2287.84 m, (b) shell deposition, 2287.84 m; perpendicular polarized microscope images, (c) calcite lens, 2295.56 m, (d) directionally aligned bioclasts, 2315.10 m.

causes a sudden rise in the salinity of the lake. Rivers pour freshwater into the lake when the climate is warm and humid (Jia et al., 2013; Wang et al., 2022). The amount of seawater entering the lake decreased as the scale of the marine transgression decreased during deposition of Unit B. In addition, the continuing input of freshwater further reduced the salinity. During the deposition of Unit C, the environment becomes more humid, resulting in increased input of fresh water and a further decline in salinity.

3) Paleoclimate

Elements Fe, Mn, Cr, Ni, V, and Co are usually enriched in humid climates, whereas evaporation enriches Ca, Mg, Sr, Ba, K, and Na in arid climates (Getaneh, 2002). A paleoclimate index, the *C*-value, has been developed based on the concentrations of these elements (Cao et al., 2012). The *C*-value is less than 0.2, between 0.2 and 0.4, between 0.4 and 0.6, between 0.6 and 0.8, and greater than 0.8, indicating arid, semi-arid, semi-arid to semi-humid, semi-humid, and humid environments in that order. The *C*-value is calculated as follows:

$$C = \frac{\sum[(\mathrm{Fe})+(\mathrm{Mn})+(\mathrm{Cr})+(\mathrm{Ni})+(\mathrm{V})+(\mathrm{Co})]}{\sum[(\mathrm{Ca})+(\mathrm{Mg})+(\mathrm{Sr})+(\mathrm{Ba})+(\mathrm{K})+(\mathrm{Na})]}. \quad (4)$$

The *C*-value of the first member of the Qingshankou ranges from 0.26 to 0.85, indicating that the paleoclimate fluctuates greatly, with alternating semi-humid and semi-arid transformation characteristics (Fig. 6(e)). From the bottom to the top, the *C*-value decreases and then increases, with the highest *C*-value in Unit C, where the climate is the most humid (Fig. 7(g)). Climate is a major factor influencing the sediment input from the sediment source area into the sedimentary system (Cecil, 1990) and so affects the input of terrigenous debris. When the climate of Unit C becomes warm and humid in K_2qn^1, the seasonally heavy rainfall may bring a large input of terrigenous debris (Liu et al., 2020; Wang et al., 2022).

4) Terrigenous detrital input

Titanium (Ti) is widely used as an indicator of terrigenous input and the Ti/Al ratio in particular is widely utilized as an index of terrestrial debris input (Brumsack, 2006; Hetzel et al., 2011). A Ti/Al ratio larger than 0.03 suggests a high input from terrestrial sources (Murphy et al., 2000; Chen et al., 2019).

The Ti/Al ratios in the K_2qn^1 range from 0.035 to 0.057, with an average of 0.040, indicating a relatively high terrigenous debris input. The terrigenous debris input is lowest in unit B, which basically has a stable input (Fig. 6(f)). From bottom to top, the Ti/Al ratio decreases and then increases, being highest in Unit C (the average is 0.042), indicating that the input of terrigenous debris is the highest in the upper sedimentary section of K_2qn^1 (Fig. 7(h)). At this time, seasonally heavy rainfall in Unit C may result in a large input of terrigenous debris, forming the thin layers of argillaceous siltstone and dolomite with unequal thicknesses (Fig. 4).

5) Lake water depth

The transport and enrichment of both Rb and K in water are closely related to clay content, and Rb is more likely to be adsorbed by clay minerals and move farther than K. Therefore, a higher Rb/K ratio indicates a greater depth of lake water (Meng et al., 2014; Sun et al., 2020).

The Rb/K ratio is greatest in Unit A, indicating that the lake water depth of K_2qn^1 steadily decreases from bottom to top (Fig. 7(i)). The lake water depth abruptly deepens in Unit A, reaches a peak depth, and then decreases; the lake water depth decreases slowly in both Units B and C (Fig. 6(g)). The rivers around the sag will advance toward the center of the lake when the lake depth of the Qingshankou Formation in the Gulong Sag decreases, and the terrigenous detrital materials in the deep-water sediments will increase (Wang et al., 2019). When the lake depth becomes shallow in Unit C, sedimentation is dominated by bottom currents and turbidity current transport. The occurrence of bottom currents is supported by lenticular bedding and directionally aligned bioclasts in the shale (Figs. 8(c) and 8(d)). Bottom and turbidity currents transport debris from shallow to deep water,and increase terrigenous material input (Fig. 7(h)).

5.2 Factors influencing organic matter enrichment

The depositional environment controls the organic matter enrichment in lake sediments (Bohacs, 1990; Bohacs et al., 2000):

$$\text{Organic Enrichment} = (\text{Production} - \text{Destruction})/\text{Dilution}. \quad (5)$$

From Eq. (5), it's evident that organic matter enrichment is favored by high primary productivity, good preservation conditions, and a weak dilution effect (Talbot, 1988). Recent studies have shown that several factors influence the elements in Eq. (5), including

primary productivity, redox conditions, paleosalinity, paleoclimate, and water depth (Ding et al., 2021; Hu et al., 2021).

In the past, when many indicators jointly characterized one control factor, such as primary productivity indicators P_{bio} and U_{bio}, the correlations between P_{bio} and TOC content, and between U_{bio} and TOC content had to be analyzed and then integrated. Since this is a time-consuming process, we proposed to simplify the above analysis by using the normalization coefficient method. Using the normalization coefficient approach, only the connection between the normalization coefficients and the TOC content needs to be studied. The normalization coefficient of primary productivity ($Productivity_{nor}$ for short) is the average of normalized P_{bio} and U_{bio}; the normalization coefficient of redox condition ($Redox_{nor}$ for short) is the average of normalized V/Cr and V/(V + Ni); the normalization coefficient of water salinity ($Salinity_{nor}$ for short) is the average of normalized Sr/Ba and m-value. Taking $Productivity_{nor}$ as an example:

$$Productivity_{nor} = [(P_{bio} - P_{biomin})/(P_{biomax} - P_{biomin}) + (U_{bio} - U_{biomin})/(U_{biomax} - U_{biomin})]/2, \quad (6)$$

where P_{bio} is biological phosphorus, P_{biomin} is its minimum, and P_{biomax} is its maximum; U_{bio} is biological uranium, U_{biomin} is its minimum, and U_{biomax} is its maximum.

Using the conventional crossplot approach, it was found that the influence of each single factor on organic matter enrichment was not clear (Fig. 9). This may be because organic matter enrichment in K_2qn^1 is the consequence of the integrated influence of numerous factors. Consequently an approach was used that incorporated numerous control factor indicators to jointly fit the measured TOC, and a multi-factor TOC correlation model was established. Each single element was used as an independent influencing factor when creating the correlation model since the correlation coefficients

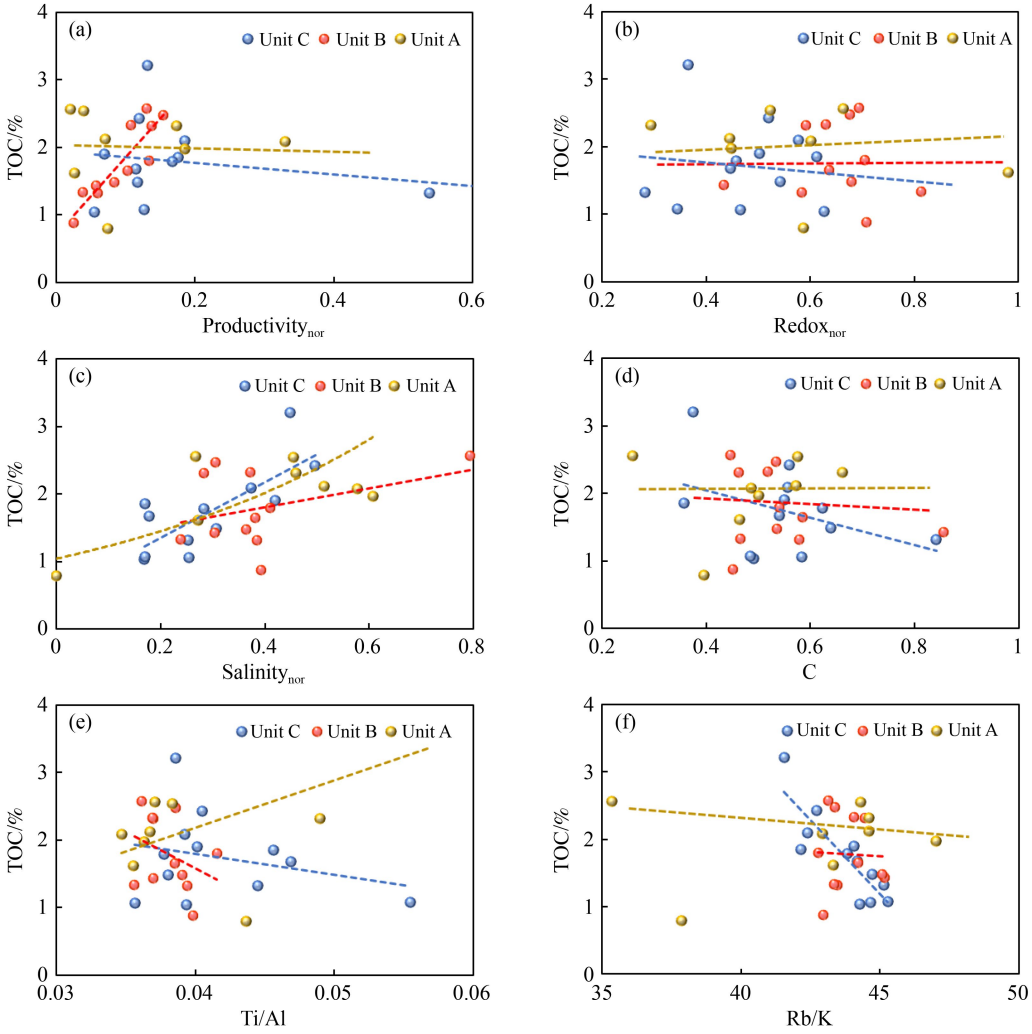

Fig. 9 No obvious correlation between (a) $Productivity_{nor}$ and TOC content, (b) $Redox_{nor}$ and TOC content, (c) $Salinity_{nor}$ and TOC content, (d) C-value and TOC content, (e) Ti/Al and TOC content, and (f) Rb/K and TOC content.

between any two factors were less than 0.7 (Fig. 10). Due to the considerable differences in the values of the control factors, the data need to be preprocessed (minimum-maximum normalization) before fitting to improve the fitting effect for comparison. Appendices C1, C2, and C3 show the normalized data results for Unit A, Unit B, and Unit C, respectively. The minimum-maximum normalization is calculated as follows:

$$X_{\mathrm{nor}} = (X - X_{\mathrm{min}})/(X_{\mathrm{max}} - X_{\mathrm{min}}), \quad (7)$$

where X is original value to be calculated, X_{nor} is normalized datum, X_{min} is minimum, and X_{max} is maximum.

In Unit A, normalized $\mathrm{Salinity_{nor}}$ is the most important control factor, followed by normalized $\mathrm{Redox_{nor}}$, normalized Ti/Al, and normalized Rb/K (Fig. 11(a)). Normalized $\mathrm{Productivity_{nor}}$ is Unit B's most essential control factor, and normalized Ti/Al follows (Fig. 11(b)). The most important control factor in Unit C is normalized Rb/K, followed by normalized $\mathrm{Salinity_{nor}}$, normalized *C*-value, and normalized $\mathrm{Redox_{nor}}$ (Fig. 11(c)). To improve the TOC correlation model's accuracy, each control factor indicator with an importance greater than 0.1 was chosen for fitting.

Unit A's TOC correlation model is as follows:

$$\mathrm{TOC_{Model}} = -0.283 + 3.522 \times \mathrm{A_1} + 1.424 \times \mathrm{A_2} + 2.417 \times \mathrm{A_3} - 1.762 \times \mathrm{A_4}, \quad (8)$$

where $\mathrm{A_1}$ is normalized $\mathrm{Salinity_{nor}}$, with larger values representing higher salinities; $\mathrm{A_2}$ is normalized $\mathrm{Redox_{nor}}$, and larger values represent stronger reduction conditions; $\mathrm{A_3}$ is normalized Ti/Al, with larger values representing higher terrigenous debris input; $\mathrm{A_4}$ is normalized Rb/K, with larger values representing deeper water depth.

Unit A's $\mathrm{TOC_{Model}}$ (fitted TOC) and $\mathrm{TOC_{Measured}}$ (measured TOC) fit well (R^2 = 0.8411; Fig. 11(d)). From the model's coefficient values, it is clear that organic matter enrichment is mainly influenced by lake water salinity in Unit A, and the marine transgression affects $\mathrm{K_2qn^1}$'s salinity-controlled organic matter enrichment. Intruding seawater supplies nutrients to Unit A, which increases primary productivity and promotes organic matter enrichment. It also causes salinity stratification, establishing a reducing environment with high salinity at the lake bottom, which is beneficial to organic matter preservation. In Unit A, organic matter enrichment is also controlled by terrigenous debris input. Talbot (1988) showed that debris input dilutes organic matter, yet a moderate input of nutrient-rich detrital material with a weak dilution effect can increase primary productivity. Moderate terrigenous debris input in Unit A weakly dilutes organic matter enrichment and brings in some terrestrial organic matter, resulting in a higher organic matter concentration. However, increased water depth generally results in longer residence times of the organic matter in the water column and higher oxic degradation, which reduces organic matter abundance.

Unit B's TOC correlation model is as follows:

$$\mathrm{TOC_{Model}} = 1.282 + 1.516 \times \mathrm{B_1} - 0.717 \times \mathrm{B_2}, \quad (9)$$

where $\mathrm{B_1}$ is normalized $\mathrm{Productivity_{nor}}$, with bigger values representing higher primary productivity; $\mathrm{B_2}$ is normalized Ti/Al.

Unit B's $\mathrm{TOC_{Model}}$ and $\mathrm{TOC_{Measured}}$ fit well (R^2 = 0.9483; Fig. 11(e)). From the model's coefficient values, it's clear that primary productivity is the main influence on the enrichment of organic matter in Unit B. The higher the primary productivity, the more the organic matter is enriched. The constant invasion of Unit B by nutrient-rich saltwater fed planktonic organisms, leading to a large increase in primary productivity. The strongly reducing environment with high salinity and high sulfur inhibits the decomposition of algae and other organisms by bacteria, and sulfate reduction occurs in large amounts of metabolizable organic matter, forming stable biopolymers (Feng et al., 2011), which ensures Unit B's good organic matter preservation. Unit B's terrigenous debris input had a weak inhibitory effect on organic matter enrichment. Discussion 5.1 shows that the terrigenous debris input in

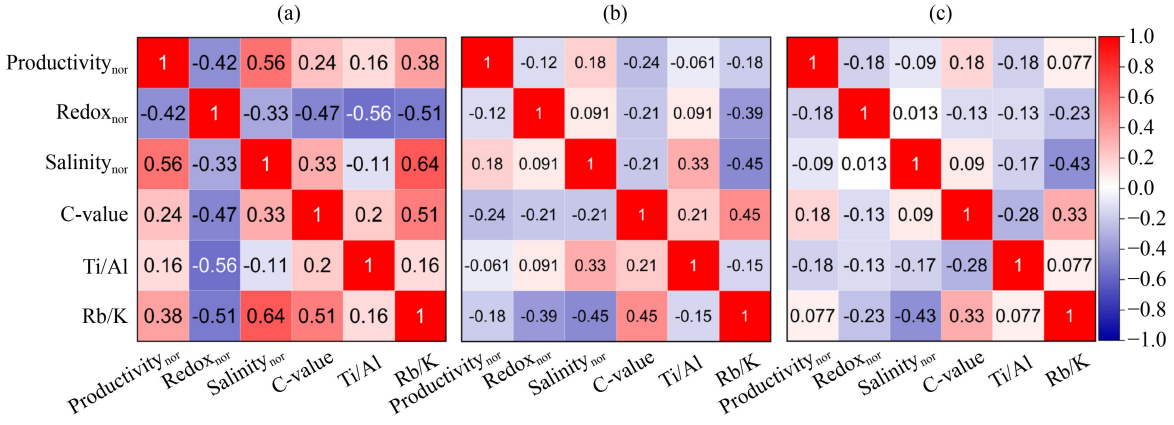

Fig. 10 The correlation plots between each single factor in (a) Unit A, (b) Unit B, and (c) Unit C.

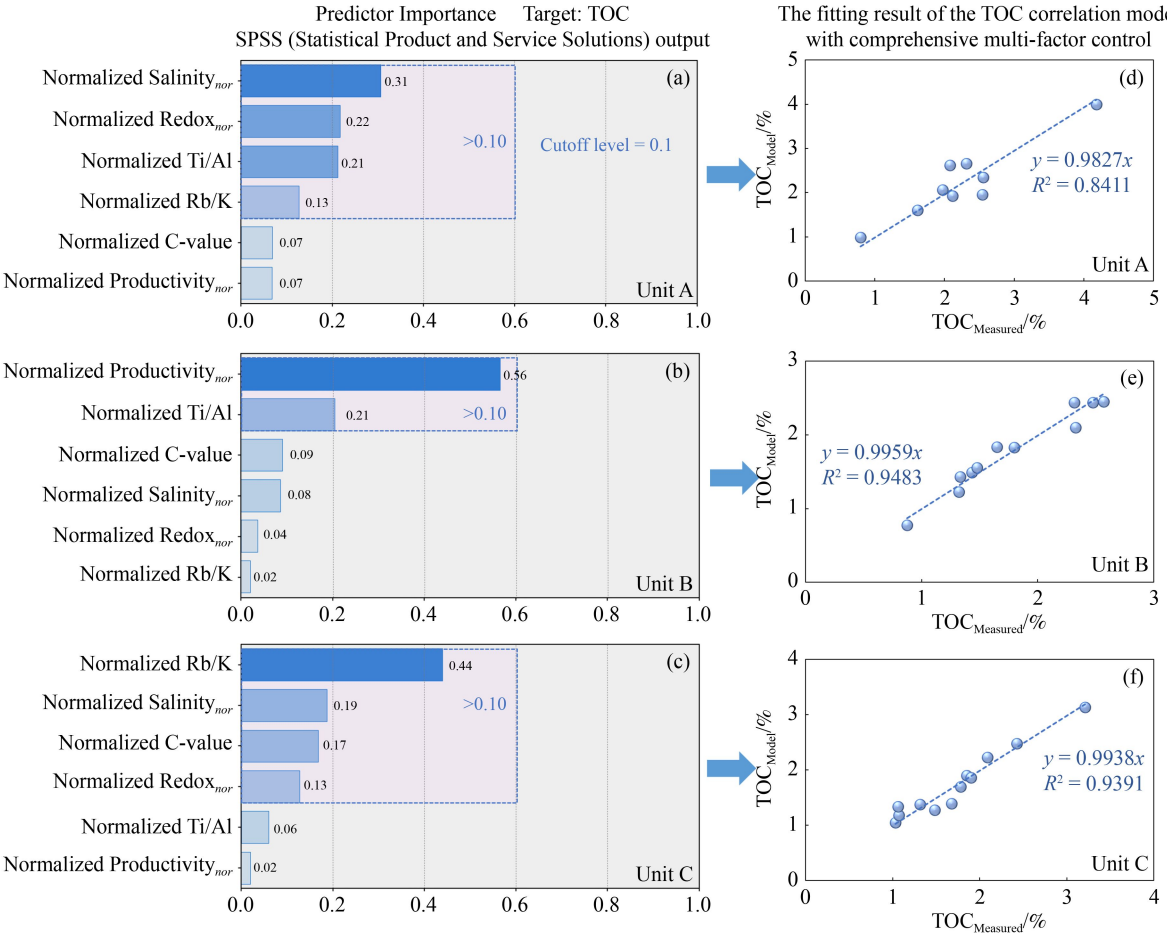

Fig. 11 Modeling control factor settings and TOC correlation model fitting.

this unit is low, therefore its inhibition effect on organic matter enrichment is weak and does not affect the enrichment of organic matter.

Unit C's TOC correlation model is as follows:

$$\mathrm{TOC_{Model}} = 2.687 - 1.345 \times C_1 + 0.704 \times C_2 - 0.597 \times C_3 - 0.207 \times C_4, \quad (10)$$

where C_1 is normalized Rb/K; C_2 is normalized Salinity$_{nor}$; C_3 is normalized Redox$_{nor}$; and C_4 is normalized *C*-value, with higher values indicating a wetter climate.

Unit C's TOC$_{Model}$ and TOC$_{Measured}$ fit well (R^2 = 0.9391; Fig. 11(f)). Unit C has the lowest organic matter content, and the model's coefficient values show that the deep water environment inhibits organic matter enrichment. Actually, increased water depth generally results in longer residence times of the organic matter in the water column and higher oxic degradation, which dilutes the organic matter concentration (Bohacs et al., 2000; Bohacs et al., 2005). In addition, the water depth in lakes is also heavily influenced by input from rivers, which are also influenced by overall rainfall levels. Thus, the humid climate that brings large amounts of rainfall also dilutes the concentration of organic matter in Unit C.

Suitable water salinity promotes biological reproduction, and fast-growing benthic organisms consume oxygen, lowering the lake's oxygen content. Simultaneously, benthic organisms' biological activity can further destabilize the previously depositional environment (Wang et al., 1994; Wang et al., 2019). Finally, in Unit C, a reducing environment disturbed by benthic organisms forms, and organic matter cannot be properly preserved, resulting in a low organic matter content. Table 1 lists the environmental characteristics of Units A, B, and C as well as their influences on organic matter enrichment.

5.3 Organic matter enrichment mechanism

A large-scale marine transgression occurred in Unit A. The invading seawater altered the lake water's physicochemical properties, such as a sudden rise in salinity, which caused many freshwater organisms to die off suddenly due to salinity intolerance. However, it also brought abundant nutrients, which caused plankton blooms, greatly enhancing primary productivity. Additionally, the injection of seawater generated density stratification, which prevented exchange between top and bottom lake waters, so the lake bottom became oxygen-

Table 1 Environmental characteristics and their effects on organic matter enrichment in K_2qn^1

Unit	TOC/%		Biotic productivity		Reducing environment		Water salinity		Warm-humid climate		Input of terrigenous debris		Water depth	
	Distribution	Average	Characteristic	Influencing of OM enrichment	Characteristic	Influencing of OM enrichment	Characteristic	Influencing of OM enrichment	Characteristic	Influencing of OM enrichment	Characteristic	Influencing of OM enrichment	Characteristic	Influencing of OM enrichment
C	0.70–2.43	1.49	High	Weak Influence	Medium	Weak Influence	Low	Promote	Strong	Weak Inhibit	Strong	Weak Influence	Shallow	Inhibit
B	0.88–2.98	1.74	Medium	Promote	Strong	Weak Influence	Medium	Weak Influence	Weak	Weak Influence	Weak	Weak Inhibit	Medium	Weak Influence
A	0.79–4.94	2.31	High	Weak Influence	Medium	Promote	High	Promote	Medium	Weak Influence	Medium	Promote	Deep	Inhibit

depleted, eventually forming black shale. Small amounts of terrestrial debris input slightly diluted the autochthonous organic matter while bringing in terrestrial organic matter, which may increase the organic matter content. The abundant organic matter was well-preserved and eventually formed the most organic-rich unit in K_2qn^1 (Fig. 12(b)).

The black laminated shale was deposited in an anoxic environment with few or no benthic organisms. The continuous deposition of black laminated shale in Unit B also demonstrates that the basin bottom was anoxic and lacked benthic life. The decrease in the scale of the marine transgression decreased the abundance of nutrients transported into the lake system. However, these nutrients can still induce plankton blooms and increase the primary productivity of the lakes. Meanwhile, invading seawater causes lake water stratification and generates strong reducing environments at the lake bottom, which preserve organic matter due to a lack of exchange between top and bottom lake water. In addition, a modest amount of terrigenous debris input will not affect the depositional environment at the lake's bottom, and an organic-rich unit will be formed in K_2qn^1 (Fig. 12(c)).

The scale of marine transgression got smaller, the lake basin area of Unit C got smaller, and the rivers surrounding the basin advanced toward the lake's center. Bottom currents and turbidity currents moved debris from shallow to deep water areas, generating numerous layers of argillaceous siltstone and dolomite with non-uniform thicknesses that separate the shale beds. River input dilutes the salinity of the lake, and benthic organisms multiply when lake salinity drops. Although the increased benthic organisms consume a huge quantity of oxygen and reduce the lake's oxygen content, their biological activities would further disrupt the previously reducing deposition environment, resulting in a reducing environment disturbed by benthic organisms. Organic matter would not be well-preserved and the unit with the lowest organic matter content in K_2qn^1 was finally formed (Fig. 12(d)).

6 Conclusions

In this work, the paleoenvironment evolutionary features in K_2qn^1 of the Gulong sag in the Songliao Basin are systematically studied, and the factors influencing the enrichment of organic matter are determined. As a result, the mechanism of organic matter enrichment in the K_2qn^1 is elucidated.

1) The cyclic variation of TOC content and elemental enrichment factor (EF) values, as well as the lithology variations, indicate that K_2qn^1 from bottom to top can be subdivided into three units, termed (from base to top) Units A, B, and C. Unit A has the highest TOC content and Unit C has the lowest. The analysis of elemental indicators shows that K_2qn^1 was deposited in a reducing brackish deep lake environment with a warm, humid climate and high primary

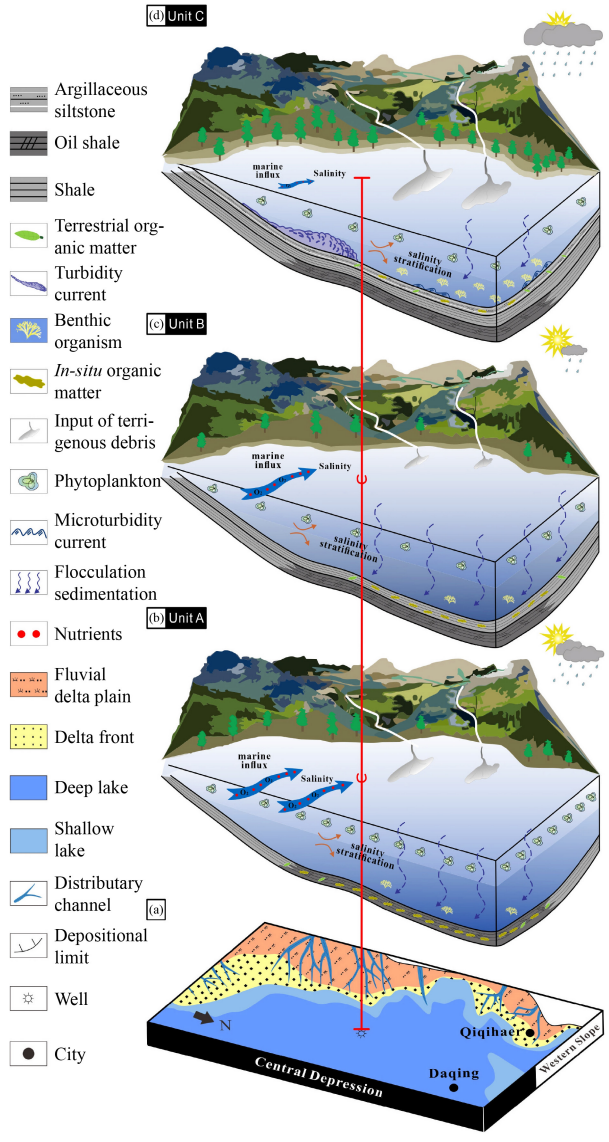

Fig. 12 Cartoon depicting the evolution of three units of K_2qn^1, Upper Cretaceous, and Songliao Basin (without scale). (a) Areal distribution of sedimentary facies; organic matter enrichment model of (b) Unit A, (c) Unit B, and (d) Unit C.

productivity. From the bottom to the top of K_2qn^1, primary productivity decreases and then increases, reducing conditions increase initially, then decrease, lake water salinity gradually decreases, the climate gets warmer and more humid, terrigenous debris input decreases and then increases, and water depth gets shallower.

2) Based on the normalization coefficients, the correlation models of organic matter enrichment demonstrate that the organic enrichment in Unit A is mainly influenced by lake water salinity, and that the strong reducing environment and moderate terrigenous debris input can also enhance it. The organic enrichment in Unit B is mainly influenced by primary productivity, and the small input of terrigenous debris has little effect. The deep water environment and humid climate in Unit C both inhibit organic matter enrichment. Even though benthic organisms reduce the oxygen content of lake water, they also destroy the environment, resulting in the poor preservation of the organic matter.

3) A large-scale marine transgression occurred at the base of K_2qn^1 (Unit A). The nutrients carried by seawater promoted primary production, and the reducing environment due to density stratification enhanced organic matter preservation, resulting in the most enriched organic matter. The middle section (Unit B) lacked benthic bioturbation, and the high primary productivity and favorable preservation conditions resulted in organic matter enrichment. The lake shallowed and the salinity decreased in the upper interval of K_2qn^1 (Unit C). Benthic organisms multiplied rapidly, destroying the previously existing environment and resulting in poor organic matter preservation conditions and the lowest organic matter content.

Acknowledgments This study was funded by the National Natural Science Foundation of China (Grant Nos. 42072147 and 41922015), and the Fundamental Research Funds for the Central Universities (No. 22CX07001A).

Appendices

Appendix A Appendix A Major element contents (%) of K_2qn^1

Depth/m	SiO_2	Al_2O_3	Fe_2O_3	CaO	Na_2O	K_2O	MgO	TiO_2	P_2O_5	MnO
2287.84	57.17	19.18	4.87	0.953	2.51	4.01	1.607	0.667	0.141	0.032
2292.2	58.686	14.69	4.56	4.897	2.972	2.59	1.887	0.592	0.28	0.116
2293.9	62.799	13.05	5.016	1.818	2.094	3.86	1.949	0.639	0.176	0.073
2295.56	46.733	18.64	7.4	4.006	2.059	3.77	1.955	0.587	1.886	0.044
2298.39	53.719	19.6	6.66	1.453	2.342	3.85	2.017	0.659	0.243	0.038
2300.6	61.144	13.9	5.729	1.886	1.825	3.98	2.173	0.575	0.158	0.051
2302.6	53.1	13.92	9.244	3.02	1.821	3.36	2.099	0.547	0.953	0.059
2309.2	55.299	16.95	7.125	3.086	2.347	3.12	2.245	0.565	0.306	0.069

(*continued*)

Depth/m	SiO_2	Al_2O_3	Fe_2O_3	CaO	Na_2O	K_2O	MgO	TiO_2	P_2O_5	MnO
2310.5	54.437	18.32	6.232	2.207	2.185	3.7	2.496	0.655	0.254	0.093
2312.2	54.68	18.81	5.9	1.635	1.999	4.05	2.207	0.652	0.199	0.048
2313.5	50.814	17.42	5.472	5.352	1.795	3.99	2.995	0.594	0.163	0.112
2315.1	54.167	17.85	6.09	2.47	2.081	3.56	2.326	0.633	0.185	0.057
2320.08	52.211	19.79	6.45	1.91	2.022	4.16	2.353	0.689	0.179	0.067
2322.89	53.28	18.79	5.37	2.654	2.246	3.97	2.323	0.661	0.117	0.059
2324.59	51.073	18.21	9.044	1.954	1.7	3.79	2.366	0.595	0.089	0.034
2326.19	55.676	20.17	4.44	0.401	1.8	4.46	2.075	0.634	0.082	0.023
2328.32	57.021	18.29	5.501	1.278	2.289	3.97	1.884	0.671	0.221	0.051
2330.62	54.112	19.27	4.95	1.657	1.768	4.32	2.269	0.629	0.15	0.069
2333.74	55.184	19.18	5.88	1.231	1.589	4.21	2.345	0.653	0.175	0.053
2339.65	56.24	19.95	5.17	0.852	1.618	4.44	2.316	0.65	0.276	0.03
2341.21	56.384	18.69	5.558	1.629	1.52	4.11	2.368	0.637	0.186	0.033
2343.06	56.094	19.52	5.292	0.766	1.425	4.52	2.483	0.674	0.193	0.051
2349.38	54.458	17.09	5.368	2.957	1.552	3.76	3.329	0.545	0.221	0.085
2350.4	55.423	21.14	4.76	0.589	1.956	4.62	2.289	0.664	0.142	0.025
2355.19	51.953	19.98	6.81	2.489	1.769	4.18	2.519	0.676	0.123	0.04
2359.32	50.148	18.74	6.82	3.305	1.56	3.99	2.362	0.608	0.281	0.062
2362.02	50.553	18.29	6.25	4.062	1.386	4.03	2.337	0.587	0.358	0.07
2363.42	61.884	12.44	5.681	2.032	1.181	4.21	2.377	0.623	0.238	0.056
2368.52	60.983	14.69	6.261	0.669	1.38	4.16	2.632	0.635	0.246	0.041
2369.92	55.69	19.19	5.01	1.405	1.55	4.62	1.931	0.588	0.659	0.052
2375.42	73.494	12.65	2.09	1.448	3.125	2.34	0.574	0.414	0.092	0.041
2377.62	64.036	15.22	4.14	3.216	2.83	2.85	1.036	0.586	0.14	0.127

Appendix B Appendix B Trace element contents (ppm) of K_2qn^1

Depth/m	Ba	V	Cr	Co	Ni	Cu	Zn	Ga	Pb	Th	Sr	Zr	Nb	U	Mo	Rb
2287.84	650.29	114.70	45.59	14.75	26.90	28.73	114.99	25.62	26.64	10.65	271.14	312.99	17.23	4.04	4.88	147.42
2292.2	607.77	78.05	33.28	12.33	17.18	25.17	80.07	19.21	27.52	11.42	555.84	254.50	14.96	4.73	4.03	90.64
2293.9	610.83	118.47	113.77	12.34	24.16	29.56	91.54	26.20	22.89	11.28	315.76	295.01	15.68	3.98	2.10	145.13
2295.56	965.79	139.10	61.29	20.52	41.55	37.63	141.94	25.31	32.54	13.97	726.52	257.38	14.38	13.17	5.34	139.76
2298.39	588.19	132.20	60.75	16.19	31.55	35.30	112.13	25.47	26.32	11.20	305.47	326.65	16.98	4.80	9.24	142.94
2300.6	860.11	119.68	82.46	13.29	23.91	30.14	137.23	26.71	25.36	11.25	309.82	299.33	14.80	4.03	5.16	146.03
2302.6	544.57	105.46	67.21	23.98	33.11	29.93	225.71	24.85	31.49	11.71	450.73	317.18	14.53	8.09	7.39	125.88
2309.2	657.91	101.12	47.52	14.05	28.68	30.60	99.15	23.47	29.01	12.39	496.15	273.38	13.51	4.90	7.57	113.51
2310.5	588.42	108.48	52.33	13.86	25.84	34.13	86.01	25.56	26.48	12.06	361.47	320.69	16.08	4.52	4.07	131.22
2312.2	615.02	126.28	54.62	15.46	29.81	43.20	102.29	27.09	30.06	13.31	328.37	326.41	16.02	6.22	16.66	142.52
2313.5	685.97	121.84	46.09	32.83	52.39	45.38	97.28	25.44	59.07	14.58	562.40	296.08	15.41	5.06	10.96	137.64
2315.1	738.74	127.16	57.09	15.62	34.25	45.56	107.04	25.58	29.61	12.51	390.06	316.44	15.53	3.80	4.70	130.24
2320.08	665.89	132.90	62.47	17.55	27.78	36.55	134.92	26.39	30.20	11.12	362.37	331.33	17.81	4.07	4.50	150.12
2322.89	711.69	143.20	56.25	15.61	27.64	37.81	113.03	24.73	31.41	13.28	374.58	330.66	16.88	3.50	7.63	141.64
2324.59	1040.53	124.96	70.67	43.91	30.99	36.39	163.58	27.14	34.74	11.43	353.98	300.89	16.34	4.17	8.12	142.14
2326.19	607.19	128.00	52.96	8.44	15.92	34.42	103.01	26.99	12.54	11.33	247.79	316.62	15.18	4.24	1.45	160.50
2328.32	707.34	117.73	46.15	14.77	22.95	29.63	98.00	26.63	27.78	11.24	304.26	307.60	16.80	4.97	6.88	141.00
2330.62	766.59	132.80	55.53	16.48	31.61	38.08	119.11	25.79	27.45	13.35	294.36	320.96	17.26	5.65	4.28	159.39
2333.74	548.30	133.70	59.16	15.51	26.21	35.93	105.48	25.94	22.47	12.67	283.58	319.30	17.19	4.81	7.11	154.55
2339.65	559.69	129.80	54.14	14.01	28.19	35.16	155.71	26.60	27.52	12.99	301.90	346.76	16.62	4.52	2.26	162.47
2341.21	1015.88	127.86	51.59	15.12	25.80	44.84	109.18	27.49	33.05	15.22	368.49	377.81	17.47	5.67	3.56	148.00
2343.06	643.37	131.63	50.71	13.84	28.33	45.01	106.13	28.87	23.32	13.91	294.39	327.23	19.30	4.41	3.40	169.14
2349.38	517.78	110.36	37.10	18.35	28.35	32.60	109.18	24.60	31.93	11.17	373.02	292.07	13.27	4.66	8.61	134.66
2350.4	598.59	159.10	49.12	9.47	21.28	50.81	121.15	28.56	12.57	13.75	256.02	361.35	17.28	3.87	4.25	166.14
2355.19	1442.99	120.50	51.21	19.94	33.08	41.05	140.52	26.42	53.45	12.44	384.74	344.66	14.98	4.01	2.65	153.74
2359.32	523.90	117.40	55.01	17.00	34.34	39.85	110.98	24.81	34.48	12.78	366.06	297.06	16.52	3.50	3.09	147.73
2362.02	546.00	115.30	58.74	16.48	30.66	35.56	143.50	24.69	26.11	12.58	462.79	319.35	11.76	5.27	5.31	157.33
2363.42	513.90	116.85	98.46	16.29	33.65	38.17	118.08	25.47	28.71	11.12	258.58	290.41	17.64	4.82	5.73	158.85
2368.52	543.02	106.00	83.02	12.89	28.08	27.47	117.67	25.53	25.37	12.01	232.42	303.26	18.72	4.87	5.44	154.01
2369.92	601.19	113.00	49.87	12.96	24.49	40.68	139.38	24.65	17.71	12.61	303.80	322.55	17.25	6.68	5.68	164.69
2375.42	725.36	39.68	22.55	4.56	4.92	3.57	34.21	13.69	14.21	7.90	209.63	202.97	8.71	2.25	0.46	68.65
2377.62	987.49	55.90	24.47	8.10	12.72	9.64	75.68	17.14	23.26	10.21	240.90	234.12	13.60	3.60	0.76	89.56

Appendix C1 Appendix C1 Normalized results in Unit A

Depth/m	TOC/ %	Original productivity	Normalized productivity	Original redox	Normalized redox	Original salinity	Normalized salinity	Original C	Normalized C	Original Ti/Al	Normalized Ti/Al	Original Rb/K	Normalized Rb/K
2350.4	1.61	0.026	0.017	0.98	1	0.272	0.448	0.464	0.511	0.036	0.039	43.32	0.683
2355.19	2.54	0.039	0.062	0.523	0.386	0.455	0.75	0.576	0.787	0.038	0.165	44.306	0.767
2359.32	2.12	0.071	0.162	0.444	0.28	0.514	0.846	0.573	0.78	0.037	0.094	44.6	0.792
2362.02	1.97	0.186	0.534	0.448	0.285	0.607	1	0.5	0.599	0.036	0.074	47.027	1
2363.42	4.18	0.192	0.556	0.236	0	0.586	0.965	0.545	0.71	0.057	1	45.452	0.865
2368.52	2.32	0.173	0.493	0.293	0.078	0.459	0.756	0.662	1	0.049	0.648	44.595	0.792
2369.92	2.08	0.33	1	0.6	0.49	0.578	0.951	0.486	0.565	0.035	0	42.941	0.65
2375.42	2.56	0.02	0	0.664	0.575	0.267	0.439	0.259	0	0.037	0.109	35.341	0
2377.62	0.79	0.074	0.174	0.586	0.47	0	0	0.395	0.339	0.044	0.406	37.856	0.215

Appendix C2 Appendix C2 Normalized results in Unit B

Depth/m	TOC/ %	Original productivity	Normalized productivity	Original redox	Normalized redox	Original salinity	Normalized salinity	Original C	Normalized C	Original Ti/Al	Normalized Ti/Al	Original Rb/K	Normalized Rb/K
2320.08	1.32	0.06	0.27	0.583	0.395	0.385	0.265	0.578	0.321	0.039	0.645	43.471	0.288
2322.89	0.88	0.025	0	0.707	0.723	0.393	0.279	0.452	0.011	0.04	0.708	42.979	0.082
2324.59	1.43	0.057	0.247	0.433	0	0.303	0.117	0.855	1	0.037	0.231	45.176	1
2326.19	1.33	0.038	0.1	0.812	1	0.238	0	0.466	0.047	0.036	0	43.35	0.237
2328.32	1.8	0.133	0.836	0.705	0.716	0.411	0.311	0.54	0.228	0.042	1	42.782	0
2330.62	2.31	0.138	0.87	0.592	0.419	0.282	0.079	0.463	0.038	0.037	0.229	44.446	0.695
2333.74	1.65	0.103	0.599	0.637	0.536	0.382	0.259	0.585	0.339	0.039	0.496	44.221	0.601
2339.65	2.33	0.108	0.641	0.63	0.518	0.372	0.24	0.518	0.174	0.037	0.218	44.079	0.542
2341.21	2.47	0.154	1	0.676	0.64	0.305	0.119	0.535	0.214	0.039	0.505	43.377	0.249
2343.06	1.48	0.084	0.456	0.678	0.646	0.365	0.228	0.535	0.215	0.039	0.584	45.076	0.958
2349.38	2.57	0.13	0.814	0.693	0.685	0.793	1	0.447	0	0.036	0.089	43.143	0.151

Appendix C3 Appendix C3 Normalized results in Unit C

Depth/m	TOC/ %	Original productivity	Normalized productivity	Original redox	Normalized redox	Original salinity	Normalized salinity	Original C	Normalized C	Original Ti/Al	Normalized Ti/Al	Original Rb/K	Normalized Rb/K
2287.84	1.03	0.055	0	0.626	1	0.169	0	0.492	0.277	0.039	0.188	44.285	0.731
2292.2	1.85	0.175	0.127	0.613	0.96	0.169	0.002	0.357	0	0.046	0.503	42.157	0.161
2293.9	1.07	0.126	0.075	0.345	0.182	0.169	0.002	0.484	0.262	0.055	1	45.291	1
2295.56	1.06	1	1	0.465	0.532	0.254	0.261	0.583	0.466	0.036	0	44.658	0.831
2298.39	1.48	0.117	0.065	0.542	0.755	0.307	0.422	0.64	0.582	0.038	0.123	44.725	0.848
2300.6	1.68	0.115	0.064	0.446	0.475	0.178	0.028	0.541	0.379	0.047	0.566	44.199	0.708
2302.6	1.32	0.538	0.511	0.282	0	0.253	0.256	0.842	1	0.044	0.445	45.129	0.957
2309.2	1.78	0.167	0.119	0.457	0.507	0.283	0.349	0.624	0.55	0.038	0.105	43.826	0.608
2310.5	2.43	0.119	0.068	0.519	0.689	0.497	1	0.559	0.416	0.04	0.244	42.721	0.312
2312.2	2.09	0.184	0.137	0.577	0.857	0.373	0.623	0.556	0.41	0.039	0.183	42.389	0.224
2313.5	3.21	0.131	0.08	0.365	0.239	0.448	0.852	0.374	0.035	0.039	0.15	41.553	0
2315.1	1.9	0.069	0.015	0.502	0.64	0.421	0.767	0.549	0.396	0.04	0.228	44.068	0.673

References

Bohacs K M (1990). Sequence stratigraphy of the Monterey Formation, Santa Barbara County: integration of physical, chemical, and biofacies data from outcrop and subsurface. AAPG Bull, 75: 139–143

Bohacs K M, Carroll A R, Neal J E, Mankiewicz P J, Gierlowski-Kordesch E, Kelts K (2000). Lake-basin type, source potential, and hydrocarbon character: an integrated sequence-stratigraphic-geochemical framework. In: Gierlowski-Kordesch, Kelts K R, eds. Lake Basins Through Space and Time. AAPG Studies in Geology, 46: 3–34

Bohacs K M, Grabowski G J, Carroll A R, Mankiewicz P J, Miskell-Gerhardt K J, Schwalbach J R, Wegner M B, Simo J T (2005). Production, destruction, and dilution—the many paths to source-rock development. SEPM Special Publications, 82: 61–101

Brumsack H J (2006). The trace metal content of recent organic carbon-rich sediments: implications for Cretaceous black shale formation. Palaeogeogr Palaeoclimatol Palaeoecol, 232(2–4): 344–361

Cao J, Wu M, Chen Y, Hu K, Bian L, Wang L, Zhang Y (2012). Trace and rare earth element geochemistry of Jurassic mudstones in the northern Qaidam Basin, northwest China. Geochem, 72(3): 245–252

Carbonel P, Colin J, Danielopol D, Löffler H, Neustrueva I (1988). Paleoecology of limnic ostracodes: a review of some major topics. Palaeogeogr Palaeoclimatol Palaeoecol, 62: 413–461

Cecil C B (1990). Paleoclimate controls on stratigraphic repetition of chemical and siliciclastic rocks. Geology, 18: 533–536

Chase Z, Anderson R F, Fleisher M Q (2001). Evidence from authigenic uranium for increased productivity of the glacial Subantarctic Ocean. Paleoceanography, 16(5): 468–478

Chen Z, Chen Z, Zhang W (1997). Quaternary stratigraphy and trace-element indices of the Yangtze Delta, Eastern China, with special reference to marine transgressions. Quat Res, 47(2): 181–191

Chen Z, Cui J, Ren Z, Jiang S, Liang X, Wang G, Zou C (2019). Geochemistry, paleoenvironment and mechanism of organic‐matter enrichment in the Lower Silurian Longmaxi Formation shale in the Sichuan Basin, China. Acta Geol Sin, 93(3): 505–519

Dill H (1986). Metallogenesis of early Paleozoic graptolite shales from the Graefenthal Horst (northern Bavaria-Federal Republic of Germany). Econ Geol, 81(4): 889–903

Ding J, Zhang J, Shi G, Shen B, Tang X, Yang Z, Li X, Li C (2021). Sedimentary environment and organic matter accumulation for the Longtan Formation shale in Xuancheng area. Acta Sediment Sin, 39: 324–340

Feng Y, Yang Z, Zhu J, Zhang S, Fu X (2021). Sequence stratigraphy in post‐rift river‐dominated lacustrine delta deposits: a case study from the Upper Cretaceous Qingshankou Formation, northern Songliao Basin, northeastern China. Geol J, 56(1): 316–336

Feng Z, Fang W, Li Z, Wang X, Huo Q, Huang C, Zhang J, Zeng H (2011). Depositional environment of terrestrial petroleum source rocks and geochemical indicators in the Songliao Basin. Sci China Earth Sci, 54(9): 1304–1317

Feng Z, Fang W, Wang X, Huang C, Huo Q, Zhang J, Huang Q, Zhang L (2009). Microfossils and molecular records in oil shales of the Songliao Basin and implications for paleo-depositional environment. Sci China Ser D Earth Sci, 52(10): 1559–1571

Feng Z, Jia C, Xie X, Shun Z, Feng Z, Cross T A (2010). Tectonostratigraphic units and stratigraphic sequences of the nonmarine Songliao Basin, northeast China. Basin Res, 22(1): 79–95

Fu X, Meng Q, Bai Y, Su Y, Jin M, Huo Z, Li H, Cui K, Xu Q, Zhu Z, Cao W, Jia Q (2022). Quantitative analysis of paleoenvironment of Qingshankou Formation in northern Songliao Basin, northeastern China. Interpretation (Tulsa), 10(3): SD75–87

Gao R Q, He C Q, Qi X Y (1992). A new genus and species of Cretaceous dinoflagellates from two transgressive beds in Songliao Basin, NE China. Acta Palaeontologica Sinica, 31: 17–29

Gao R, Cai X (1997). Hydrocarbon Formation Conditions and Distribution Rules in the Songliao Basin. Beijing: Petroleum Industry Press, 1–103

Getaneh W (2002). Geochemistry provenance and depositional tectonic setting of the Adigrat Sandstone northern Ethiopia. J Afr Earth Sci, 35(2): 185–198

Guan M, Wu S, Hou L, Jiang X, Ba D, Hua G (2021). Paleoenvironment and chemostratigraphy heterogeneity of the Cretaceous organic-rich shales. Adv Geo-Energy Res, 5(4): 444–455

Haddad R I, Martens C S (1987). Biogeochemical cycling in an organic-rich coastal marine basin: 9. Sources and accumulation rates of vascular plant-derived organic material. Geochim Cosmochim Acta, 51(11): 2991–3001

Hakimi M H, Abdullah W H, Shalaby M R, Alramisy G A (2014). Geochemistry and organic petrology study of Kimmeridgian organic-rich shales in the Marib-Shabowah Basin, Yemen: origin and implication for depositional environments and oil-generation potential. Mar Pet Geol, 50: 185–201

Hetzel A, März C, Vogt C, Brumsack H J (2011). Geochemical environment of Cenomanian-Turonian black shale deposition at Wunstorf (northern Germany). Cretac Res, 32(4): 480–494

Hou D (1999). The characteristics of molecular geochemistry of marine transgression strata in Songliao Basin. Acta Petrol Sin, 20: 30–34

Hou D, Feng Z, Huang Q (2003). Geological and geochemical evidences of anoxic event in the Songliao Basin. Geoscience, 17: 311–317

Hu T, Pang X, Jiang F, Wang Q, Xu T, Wu G, Cai Z, Yu J (2021). Factors controlling differential enrichment of organic matter in Saline Lacustrine Rift Basin: a case study of third member Shahejie Fm in Dongpu Depression. Acta Sedimento Sin, 39: 140–152

Huang Q, Zheng Y, Yang M, Li X, Han M, Chen C (1999). On Cretaceous paleoclimate in the Songliao Basin. Acta Micropalaeontologica Sin, 16: 95–103

Jarvie D M (2012). Shale resource systems for oil and gas: part 2—Shale-oil resource systems. In: Breyer J A, ed. Shale Reservoirs—Giant Resources for the 21st Century. AAPG Memoir, 97: 89–119

Jenkyns H C (1980). Cretaceous anoxic events: from continents to oceans. J Geol Soc London, 137(2): 171–188

Jia J, Liu Z, Bechtel A, Strobl S A, Sun P (2013). Tectonic and climate

control of oil shale deposition in the Upper Cretaceous Qingshankou Formation (Songliao Basin, NE China). Int J Earth Sci, 102(6): 1717–1734

Jones B, Manning D A (1994). Comparison of geochemical indices used for the interpretation of palaeoredox conditions in ancient mudstones. Chem Geol, 111(1–4): 111–129

Li C, Yan W, Wu H, Tian H, Zheng J, Yu J, Feng Z, Xu H (2022). Calculation method of oil saturation in clay-rich shale reservoirs and its application: a case study of Qing 1 Member of Cretaceous Qingshankou Formation in Gulong Sag, Songliao Basin, NE China. Pet Explor Dev, 49: 1–11

Li D (1996). Basic characteristics of oil and gas basins in China. J Southeast Asian Earth Sci, 13(3–5): 299–304

Liu B, Shi J, Fu X, Lyu Y, Sun X, Gong L, Bai Y (2018). Petrological characteristics and shale oil enrichment of lacustrine fine-grained sedimentary system: a case study of organic-rich shale in first member of Cretaceous Qingshankou Formation in Gulong Sag, Songliao Basin, NE China. Pet Explor Dev, 45(5): 884–894

Liu B, Song Y, Zhu K, Su P, Ye X, Zhao W (2020). Mineralogy and element geochemistry of salinized lacustrine organic-rich shale in the Middle Permian Santanghu Basin: implications for paleoenvironment, provenance, tectonic setting and shale oil potential. Mar Pet Geol, 120: 104569

Liu B, Wang H, Fu X, Bai Y, Bai L, Jia M, He B (2019). Lithofacies and depositional setting of a highly prospective lacustrine shale oil succession from the Upper Cretaceous Qingshankou Formation in the Gulong sag, northern Songliao Basin, northeast China. AAPG Bull, 103(2): 405–432

Liu B, Wang Y, Tian S, Guo Y, Wang L, Yasin Q, Yang J (2022). Impact of thermal maturity on the diagenesis and porosity of lacustrine oil-prone shales: insights from natural shale samples with thermal maturation in the oil generation window. Int J Coal Geol, 261: 104079

Meng X, Li C, Gui R (2014). Ancient sedimentary environment significance revealed by the trace elements of Shan 2 to He 8 member of Upper Paleozoic in Yanan. Unconventional Oil & Gas, 1: 26–30

Murphy A E, Sageman B B, Hollander D J, Lyons T W, Brett C E (2000). Black shale deposition and faunal overturn in the Devonian Appalachian Basin: clastic starvation, seasonal water‐column mixing, and efficient biolimiting nutrient recycling. Paleoceanography, 15(3): 280–291

Peters K, Moldowan J, Schoell M, Hempkins W (1986). Petroleum isotopic and biomarker composition related to source rock organic matter and depositional environment. Org Geochem, 10(1–3): 17–27

Rimmer S M (2004). Geochemical paleoredox indicators in Devonian–Mississippian black shales, central Appalachian Basin (USA). Chem Geol, 206(3–4): 373–391

Rimmer S M, Thompson J A, Goodnight S A, Robl T L (2004). Multiple controls on the preservation of organic matter in Devonian–Mississippian marine black shales: geochemical and petrographic evidence. Palaeogeogr Palaeoclimatol Palaeoecol, 215(1–2): 125–154

Song Y, Liu Z, Meng Q, Xu J, Sun P, Cheng L, Zheng G (2016). Multiple controlling factors of the enrichment of organic matter in the upper cretaceous oil shale sequences of the Songliao Basin, NE China: implications from geochemical analyses. Oil Shale, 33(2): 142–166

Sun L, Liu H, He W, Li G, Zhang S, Zhu R, Jin X, Meng S, Jiang H (2021). An analysis of major scientific problems and research paths of Gulong shale oil in Daqing Oilfield, NE China. Pet Explor Dev, 48(3): 527–540

Sun Z, Wang F, Hou Y, Luo J, Zheng Y, Wu S, Zhu G (2020). Main controlling factors and modes of organic matter enrichment in salt lake shale. Earth Sci (Paris), 45: 1375–1387

Talbot M (1988). The origins of lacustrine oil source rocks: evidence from the lakes of tropical Africa. Spec Publ Geol Soc Lond, 40(1): 29–43

Taylor S R, McLennan S M (1985). The Continental Crust: Its Composition and Evolution: An Examination of the Geochemical Record Preserved in Sedimentary Rocks. Oxford: Blackwell Scientific

Tribovillard N, Algeo T J, Lyons T, Riboulleau A (2006). Trace metals as paleoredox and paleoproductivity proxies: an update. Chem Geol, 232(1–2): 12–32

Vincent B, Rambeau C, Emmanuel L, Loreau J P (2006). Sedimentology and trace element geochemistry of shallow-marine carbonates: an approach to paleoenvironmental analysis along the Pagny-sur-Meuse Section (Upper Jurassic, France). Facies, 52(1): 69–84

Wang D, Liu Z, Liu L (1994). Evolution and Sea Level Elevation of Songliao Basin. Beijing: Geological Publishing House, 91–128 (in Chinese)

Wang F, Liu X, Deng X, Li Y, Tian J, Li S, You J (2017). Geochemical characteristics and environmental implications of trace elements of Zhifang Formation in Ordos Basin. Acta Sedimentologica Sinica, 35: 1265–1273

Wang L, Zeng W, Xia X, Zhou H, Bi H, Shang F, Zhou X (2019). Study on lithofacies types and sedimentary environment of black shale of Qingshankou Formation in Qijia-Gulong Depression, Songliao Basin. Nat Gas Geosci, 30: 1125–1133

Wang L, Zhou H, Shang F, Zhou X (2022). Element geochemical characteristics of black shale and paleo-sedimentary environmental restoration of Qingshankou Formation of the Cretaceous in the northern Songliao Basin. Chinese J Geo, 57: 156–171

Wang P, Wang D, Du X (1996). The origin of the black shales and the bottom current model for seawater encroachment in the Cretaceous Qingshankou Formation, Songliao Basin, northeast China. Sediment Facies Palaeogeogr, 16: 34–43

Wang Y, Liu Z, Sun P (2015). Organic matter evolution in the first member of Qingshankou Formation in Well NGN1, Upper Cretaceous, Songliao Basin. Global Geo 34: 735–742 (in Chinese)

Wignall P B (1994). Black Shales. Oxford Monographs on Geology and Geophysics 30. New York: Oxford University Press

Wu H, Zhang S, Huang Q (2008). Establishment of floating astronomical time scale for the terrestrial Late Cretaceous Qingshankou Formation in the Songliao Basin of northeast China. Earth Sci Front, 15(4): 159–169

Wu H, Zhang S, Jiang G, Huang Q (2009). The floating astronomical

time scale for the terrestrial Late Cretaceous Qingshankou Formation from the Songliao Basin of northeast China and its stratigraphic and paleoclimate implications. Earth Planet Sci Lett, 278(3–4): 308–323

Xu C, Shan X, He W, Zhang K, Rexiti Y, Su S, Liang C, Zou X (2021). The influence of paleoclimate and a marine transgression event on organic matter accumulation in lacustrine black shales from the Late Cretaceous, southern Songliao Basin, northeast China. Int J Coal Geol, 246: 103842

Xu J, Liu Z, Bechtel A, Meng Q, Sun P, Jia J, Cheng L, Song Y (2015). Basin evolution and oil shale deposition during Upper Cretaceous in the Songliao Basin (NE China): implications from sequence stratigraphy and geochemistry. Int J Coal Geol, 149: 9–23

Yang D, Yu M (2002). The Uranium-organic geochemistry development. Global Geo, 21: 18–23

Zhang C, Zhang W, Guo Y (2012). Sedimentary environment and its effect on hydrocarbon source rocks of Longmaxi Formation in Southeast Sichuan and Northern Guizhou. Earth Sci Front, 19: 136–145

Zhang S (1988). Research and application of Magnesium-Aluminum content ratio in sedimentary rock. Bulletin of Mineralogy, Petrology Geochem, 7: 112–113 (in Chinese)

Zhao Z, Littke R, Zieger L, Hou D, Froidl F (2020). Depositional environment, thermal maturity and shale oil potential of the Cretaceous Qingshankou Formation in the eastern Changling Sag, Songliao Basin, China: an integrated organic and inorganic geochemistry approach. Int J Coal Geol, 232: 103621

Zheng G, Meng Q, Liu Z (2020). Geochemical characteristics and paleolimnological information of oil shale in 1st member of Qingshankou Formation in Northern Songliao Basin. J Jilin U Earth Sci Ed, 50: 392–404

Zou C, Zhu R, Chen Z, Ogg J G, Wu S, Dong D, Qiu Z, Wang Y, Wang L, Lin S, Cui J, Su L, Yang Z (2019). Organic-matter-rich shales of China. Earth Sci Rev, 189: 51–78